THE ASTROPHYSICAL JOURNAL, 344:876–888, 1989 September 15

THE MAGNETIC FIELD AND ABUNDANCE DISTRIBUTION GEOMETRY OF THE PECULIAR B STAR HD 215441

J. D. LANDSTREET,[1] P. K. BARKER, D. A. BOHLENDER, AND M. S. JEWISON[1]
Department of Astronomy, University of Western Ontario
Received 1988 October 3; accepted 1989 February 24

ABSTRACT

Nine high-resolution, high signal-to-noise spectra of the strongly magnetic Bp star HD 215441 = Babcock's star, well spaced through the rotation cycle, have been obtained. These data have been used to model the magnetic field geometry of the star and the distribution over one hemisphere of the elements Si, Ti, Cr, and Fe by means of a line synthesis program that includes the effects of the magnetic field and of nonuniform abundance distributions.

The magnetic field axis appears to be inclined to the rotation axis at an angle of about 35°, and the rotation axis is inclined to the line of sight by about the same amount. The Zeeman splitting of spectral lines is reasonably well reproduced by an axisymmetric superposition of dipole, quadrupole, and octupole of polar strengths +67, −55, and +30 kG, respectively.

The abundance distributions are assumed to be axisymmetric about the magnetic axis. The elements Si, Ti, Cr, and Fe appear to have overabundances (relative to the Sun) around the magnetic equator of roughly 1.5, 2.3, 1.9, and 0.5 dex, respectively, and all four elements are about 1 dex more abundant around the visible positive pole than around the magnetic equator.

Subject headings: stars: abundances — stars: individual (HD 215441) — stars: magnetic — stars: peculiar A — Zeeman effect

I. INTRODUCTION

In 1959 Babcock (1960) discovered an extremely large magnetic field in the Ap Si star HD 215441 (=Babcock's star). In fact, the field is large enough to split most of the lines in the spectrum into Zeeman patterns in which groups of π and σ components are resolved. From the degree of splitting observed, Babcock was able to estimate that the magnitude B_s of the photospheric magnetic field in this star must be about 34 kilogauss.

It is unusual to observe resolved Zeeman patterns in magnetic A and B stars. Only a very small number of stars combine the extremely large fields ($\gtrsim$10 kG) and very low projected rotational velocities ($\lesssim$10 km s^{-1}) necessary for this effect to be observable; at present, only about a dozen stars showing resolved lines are known (Preston 1969*a*, *b*, 1971*a*; Didelon 1988). HD 215441 was the first star found to exhibit this effect, and its discovery stimulated a great deal of interest. However, the star is quite faint ($V \approx 8.84$), and so it has been extensively studied only by means of broad-band photoelectric photometry.

Large photometric variations, with amplitude exceeding 0.1 mag in the Johnson *U*, *B*, and *V* bands, were first detected by Jarzębowski (1960), who found a stellar rotation period of 9.49 days. A number of other groups have subsequently studied the light variations; references may be found in the very useful bibliographies of Catalano and Renson (1984, 1987).

Light variations of Babcock's star in the ultraviolet were studied by Leckrone (1974). He found that the star is brightest at wavelengths shorter than 2460 Å when it is faintest at longer wavelengths, and vice versa. Leckrone interpreted his observations as revealing variable blanketing and backwarming, so that the large light variations are due to variations in atmospheric structure over the star rather than to variations in local effective temperature. In fact, Leckrone argued that T_e varies by no more than $\sim \pm 100$ K, and may well be constant. He estimated $T_e \approx 14{,}500$ K; he also combined all available photometry up to that time to establish an accurate ephemeris for the variations.

Preston (1969*a*) obtained a series of spectra through the 9.5 day cycle. He showed that the Zeeman splitting of the resolved lines varies slightly through the period, with the mean surface field varying between values of about 34 kG at maximum light and 32 kG at minimum. Neither Preston nor Babcock was successful at measuring the longitudinal component of the field by the usual photographic technique; too many of the lines are completely resolved.

Preston (1969*a*) also made the first attempt to model the magnetic field geometry of Babcock's star, using the oblique rotator model (e.g., Preston 1971*b*). From the observed period and projected rotational velocity $v \sin i \approx 5$ km s^{-1}, he found that the inclination i of the rotation axis to the line of sight is $i < 30°$. An examination of the phase variation of the relative strengths of the σ_+ and σ_- components on his (Zeeman analyzed) plates then showed that the line of sight to the star never goes farther than about 70° from one magnetic pole, if the field may be approximately described as a (centered) dipole. This implies that the angle β between the magnetic and rotation axis is $\beta < 40°$. However, Preston was unable to reproduce the observed ratio of strengths of the σ_+ to σ_- components using a dipole model, and came to the important conclusion that the field geometry of HD 215441 must depart significantly from that of a simple centered dipole.

Babcock and Preston had both noted that the spectrum of HD 215441, while not obviously variable, does change subtly. These spectrum variations were studied by Krautter (1977), who measured equivalent widths on Preston's 8 Å mm^{-1} Lick

[1] Visiting Astronomer, Canada-France-Hawaii Telescope, operated by the National Research Council of Canada, the Centre National de la Recherche Scientifique of France, and the University of Hawaii.

plates. Krautter found that virtually all observed lines on those plates are periodically variable with the rotation period of the star, and that all the strong (saturated) lines readily measured are about 1.5 times stronger at maximum V light than at minimum V light. He argued that these variations are too large to be due to effects of the magnetic field, but must reflect abundance variations over the stellar surface. (Because all lines increase and decrease in strength together, the visual appearance of the photographic spectrum changes rather little with phase.)

In 1975, Borra and Landstreet (1978) measured the longitudinal field component B_l as a function of rotation phase with a photoelectric Balmer-line Zeeman analyzer. B_l is found to vary periodically from about +20,500 G at maximum V light to about +10,900 G at minimum V light. The lack of sign change confirms Preston's contention that the line of sight stays within about 70° of one magnetic pole. Borra and Landstreet attempted to model the magnetic field geometry of HD 215441 using a decentered dipole model (Landstreet 1970) that seems to provide a first-order description of most magnetic A and B stars (cf. Landstreet 1980). They found that they could approximately account for both Preston's and their own magnetic measurements with $i \approx \beta \approx 30°$–$35°$ and a dipole decentered by about 0.2 to 0.3 stellar radii, with a polar field of about 33 to 35 kG at the weaker positive (observed) pole and a field of ~ -120 to -210 kG at the unobserved strong pole. Attempts to use this magnetic model to make approximate line profile calculations using the simple Unno (1956) theory of line formation led to calculated intensity profiles in qualitative agreement with Preston's observations, but did not correctly account for the strength ratios of σ_+/π and π/σ_- observed by Preston. Nevertheless, the decentered dipole model seems to be an improved description of the field geometry of Babcock's star, even though there are suggestions that it is not exact.

Over the past few years, one of us (J. D. L.) has been engaged in a comprehensive effort to model both magnetic field geometries and photospheric abundance distributions for a number of Ap and Bp magnetic stars. The goal of this project is to obtain models that establish without too much ambiguity the relationship between the magnetic field geometry and the abundance distributions, so that the models can provide genuinely useful stimulus to and tests of theories of how the observed abundance patches and field configurations have been produced. A model of one star, 53 Cam = HD 65339, has already been described (Landstreet 1988); further discussion about modeling techniques and philosophy can be found in that paper.

As part of this program, we obtained a new series of high-resolution, high signal-to-noise spectra of HD 215441, well spaced through the rotation period. In this paper, we discuss models of the magnetic geometry and of the distributions over the stellar surface of Si, Ti, Cr, and Fe that may be derived from this material. In the next section, we discuss the new data; in § III, modifications to the line synthesis program used for modeling are described; § IV discusses how the magnetic field geometry and the abundance distributions are determined. A final section draws some further conclusions and summarizes results.

II. OBSERVATIONS

For this project, new spectra of HD 215441 were obtained in 1983 August using the coudé spectrograph of the Canada-France-Hawaii Telescope with the 1872 diode Reticon array. The 830 line per mm grating was used in second order, providing a resolution of 0.10 Å. To obtain full phase coverage through the 9.49 day period, our six assigned nights were pooled with three nights assigned to A. M. Boesgaard and spectra were obtain on all nine nights. Because HD 215441 is quite faint, an exposure of about 3 hr was necessary to reach the desired signal-to-noise ratio of around 300, which required about half of our part of each night. As we also wished to obtain spectra of standard stars and some other Ap stars, we were able to observe only one 65 Å spectral region each night. After examining the line lists of Preston (1969*a*) and Adelman (1974), the spectral window 4532–4597 Å was selected, as this interval contains several lines of each of Cr II, Fe II, Si III, and Ti II. The available lines in this window do not have a very large range in magnetic sensitivity (z-value), but because most lines in this star are resolved into Zeeman patterns, this is not important. More significantly, the unblended Cr, Fe, and Ti lines cover a large range in strength, so that abundances can be derived using fairly weak lines.

Phases were calculated using the ephemeris of Leckrone (1974),

$$\text{JD (max light } \lambda > 3300 \text{ Å)} = 2436864.88 + 9.4871E \; . \quad (1)$$

A slightly longer period of 9.4875 days is preferred by Hempelmann and Schöneich (1983); a somewhat shorter one of 9.4866 days by Schöneich, Hildebrandt, and Furtig (1976). If we assume that this difference is a reasonable measure of the uncertainty of the period, the phases of our spectral observations are uncertain relative to the Balmer line magnetic measurements of Borra and Landstreet (1978) by only ~ 0.02, a value small enough not to affect the analysis significantly. (Relative to the zero point of Leckrone's ephemeris, phases are uncertain by ~ 0.04.) A journal of observations is given in Table 1, which lists in successive columns the Julian date at the midpoint of obervations, the duration of the full exposure in minutes, and the phase of the observation. It will be seen that the phase coverage of these new spectra is excellent.

The spectra were reduced using a package of programs written by one of us (P. K. B.) in a manner similar to the reductions done for 53 Cam (Landstreet 1988). The scale of pixel number versus wavelength is determined by fitting observations of an Fe–Ar or a Th–Ne hollow cathode lamp with a cubic polynominal. The stellar spectra are then corrected for pixel-to-pixel sensitivity variations by division by the sum of four flat-field lamp spectra, each of which is exposed to about the same level as the stellar continuum. The slope of the continuum produced by division of the spectrum of the hot star by

TABLE 1

JOURNAL OF SPECTRAL OBSERVATIONS OF HD 215441

Julian Date (2,445,500+)	Duration (minutes)	Phase
65.006.....	167	0.048
65.999.....	172	0.153
67.008.....	228	0.259
67.972.....	167	0.361
68.987.....	167	0.468
69.973.....	170	0.572
70.975.....	191	0.677
71.976.....	189	0.783
72.969.....	160	0.887

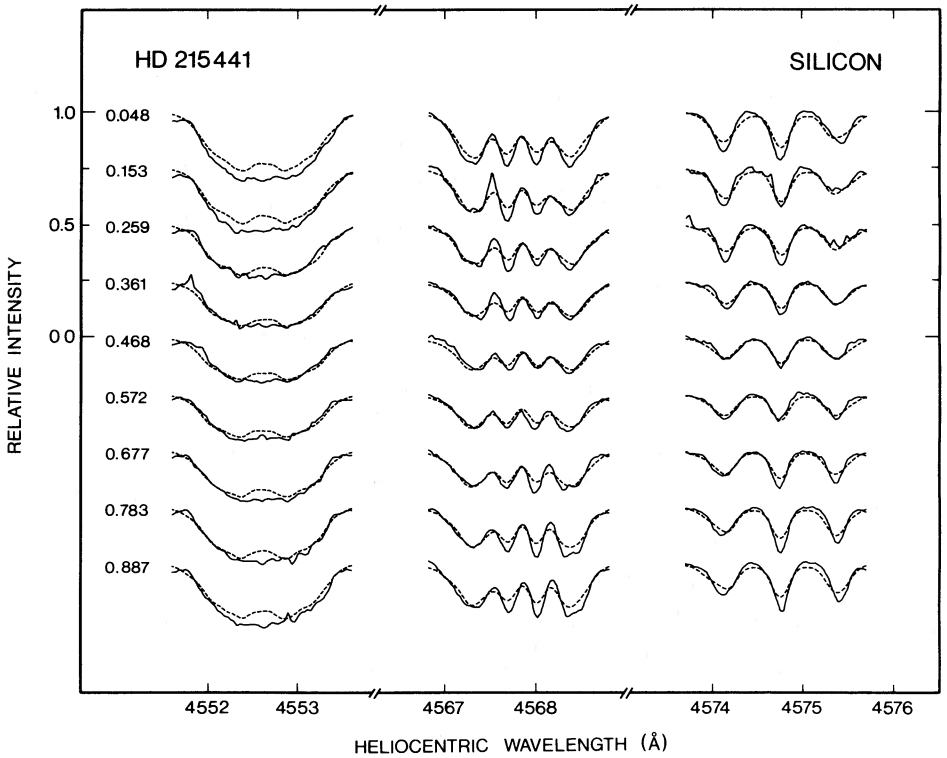

FIG. 1.—Observed profiles (*solid curves*) of several lines in the spectrum of HD 215441 that are primarily due to Si. The nine rows are from spectra obtained at nine successive rotational phases of the star (see Table 1). The phases are indicated in the left margin; the top spectrum corresponds nearly to passage of the positive magnetic pole through the subsolar point ($\alpha \approx 0°$) and phase 0.468 is close to the phase of nearest approach to the magnetic equator ($\alpha \approx 70°$). The lines are identified along the bottom margin. Each segment is approximately 2 Å wide. The dashed curves are model profiles calculated with the magnetic geometry described in the text and the abundance distributions of Table 3. All blending lines listed in Table 2 are included in the calculation.

that of a cool lamp, and residual waves in the continuum (cf. Landstreet 1988), are removed by fitting a sixth-order polynominal to a number of continuum points in a single spectrum and then dividing that spectrum by the polynominal. This procedure leads to continua that are within about ± 0.01 or 1.00. All spectra are corrected to a heliocentric wavelength scale.

Several spectral lines of each element studied are shown in Figures 1 (lines of Si), 2 (Ti), 3 (Cr), and 4 (Fe). In each figure, a single row is composed of spectral lines extracted from a single spectrum; successive rows are from spectra at successive phases as listed in Table 1, starting with phase 0.048. The observed spectra are shown as solid curves; model spectra (described in § IV below) are drawn dashed. Atomic data for the modeled lines are listed in Table 2. For each spectral feature modeled, this table contains the element, multiplet number, and wavelength of each of the individual atomic lines that we believe contribute significantly to the feature. Wavelengths are taken from the Revised Multiplet Table (Moore 1945). The features are grouped by the principal element responsible. To aid in understanding Figures 1–4, the Zeeman pattern of each contributing line is also given, with π components in parentheses. The last three columns contain log *gf*-values, first from Kurucz and Peytremann (1975) or Kurucz (1981), then from the best available experimental source, with a letter grade if the experimental value has been evaluated by the National Bureau of Standards (Martin, Fuhr, and Wiese 1988), a footnote indicating the original source of the measurement, and finally our adopted value. The rationale for the adopted log *gf*-values will be discussed in § IV.

III. MODELING TECHNIQUES

The basic approach to modeling taken here is to calculate the expected profiles of individual spectral lines for an assumed magnetic field geometry and abundance distribution with the aid of a line synthesis program that takes into account the effects of the large magnetic field. The calculated profiles are compared with those observed at various phases, and the model field geometry and abundance distributions are altered until acceptable agreement with observation is obtained.

The line synthesis program used has been described in some detail by Landstreet (1988). Line profiles are calculated assuming an atmosphere structure taken from models available in the literature. The lines are assumed to be formed in LTE and pure absorption. Turbulence in the atmosphere is assumed to be suppressed by the magnetic field, and the microturbulence is set to zero (this will be discussed further below). The magnetic splitting of each line in response to a specified local magnetic field is calculated assuming LS coupling, and the absorption and polarization effects due to each Zeeman component are included separately at the appropriate wavelengths. The coupled equations of transfer describing the propagation of polarized light through a magnetized atmosphere (Unno 1956; Hardorp, Shore, and Wittmann 1976) are solved (in the approximation that anomalous dispersion is neglected) at typically 60 points on the observed stellar hemisphere using the efficient method of Martin and Wickramasinghe (1979); the resulting local line profiles are transformed to the global frame of reference of the star and added (with appropriate Doppler

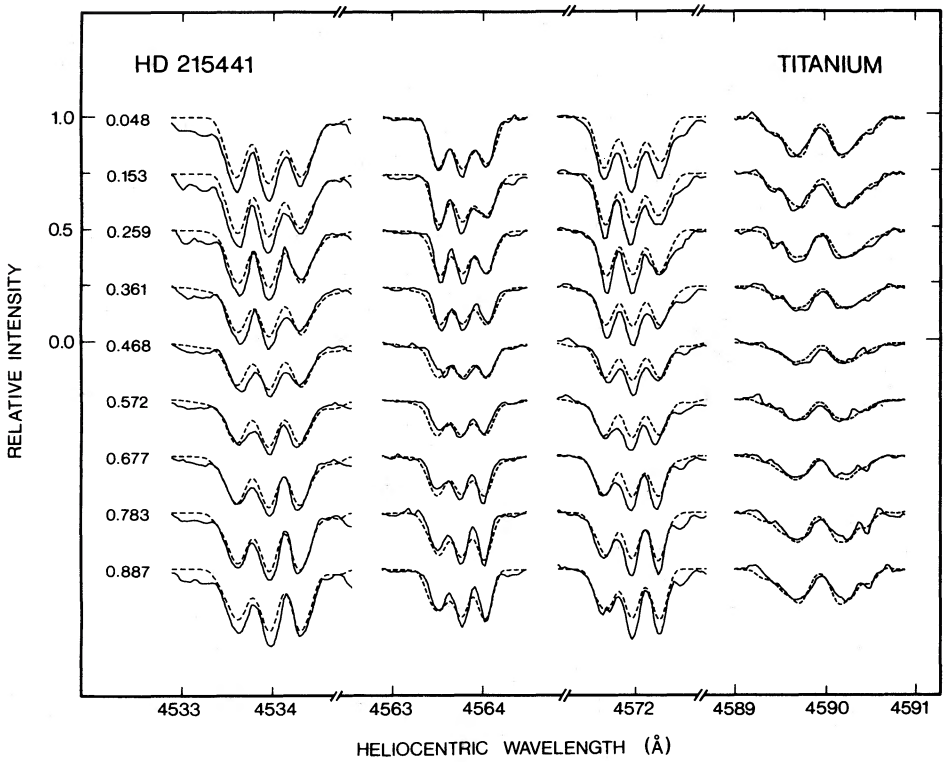

FIG. 2.—Same as Fig. 1, for lines primarily due to Ti

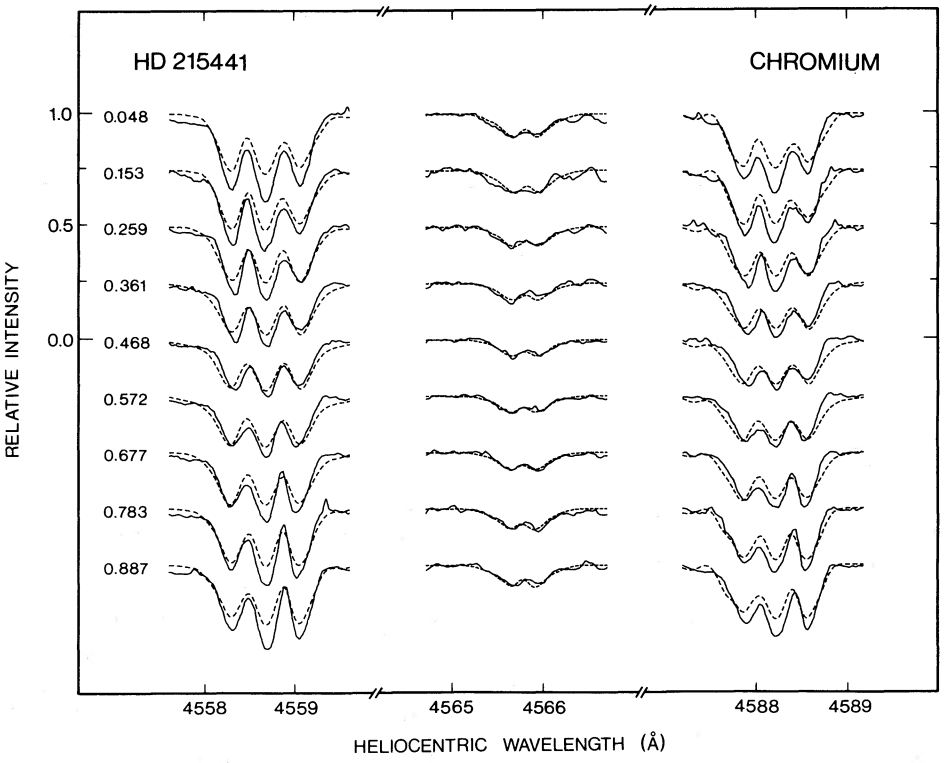

FIG. 3.—Same as Fig. 1, for lines primarily due to Cr

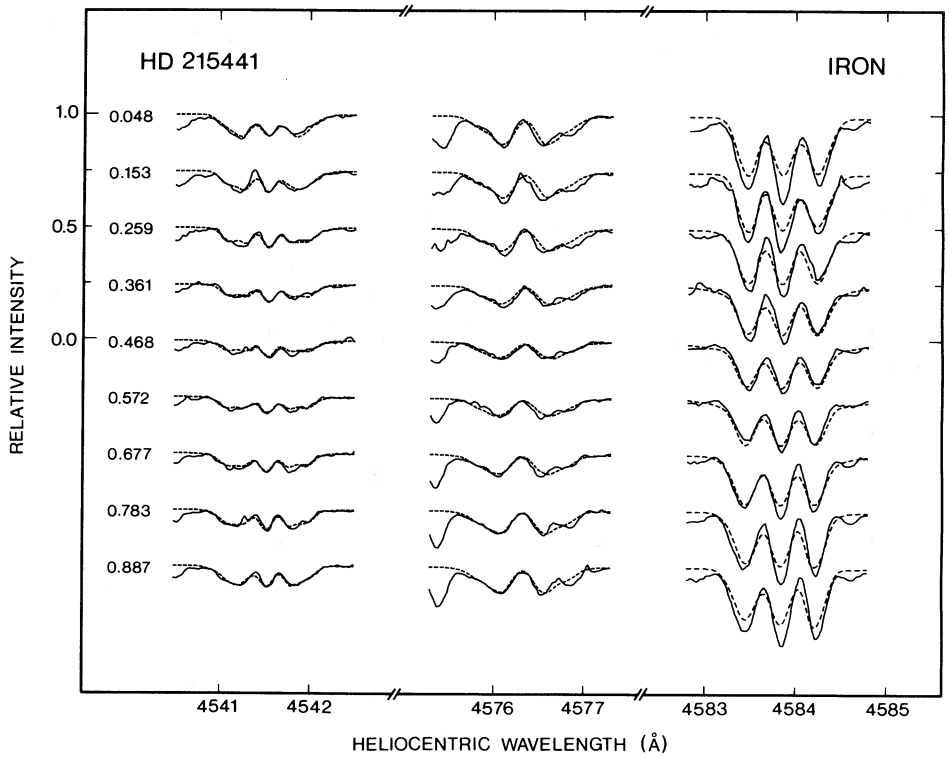

FIG. 4.—Same as Fig. 1, for lines primarily due to Fe

TABLE 2

SPECTRAL LINES MODELED

ION (mult)	WAVELENGTH (Å)	ZEEMAN PATTERN	LOG *gf* KP/K	LOG *gf* Obs.	Ref.	Adopt
Si III(2)	4552.654	(0.00, 0.50) 1.00, 1.50, 2.00	0.33	0.29C	1	0.29
Si III(2)	4567.841	(0.50) 1.50, 2.00	0.10	0.07C	1	0.07
Si III(2)	4574.757	(0.00) 2.00	−0.38			−0.41
Ti II(50)	4533.966	(0.07,'0.20) 1.00, 1.13, 1.27, 1.40	−0.70	−0.77D	2	−0.77
Fe II(37)[a]	4534.166	(0.31, 0.94) 0.09, 0.71, 1.34, 1.97	−3.33	−3.47D	2	−3.47
Ti II(50)	4563.761	(0.07) 0.73, 0.87	−0.86	−0.96D	2	−0.96
Ti II(82)	4571.971	(0.01, 0.03, 0.05, 0.07) 0.84, 0.86, ..., 0.98	−0.32	−0.53D	2	−0.53
Cr II(44)[a]	4589.89	(0.49, 1.46) −0.09, 0.89, 1.86, 2.83	−2.64	−1.82	3	−2.42
Ti II(50)	4589.961	(0.27, 0.80) 0.53, 1.07, 1.60	−1.72	−1.79D	2	−1.79
Cr II(44)	4558.659	(0.05, 0.14, 0.24, 0.33) 1.00, 1.10, ..., 1.67	−0.69	+0.18	3	−0.42
Cr II(44)[a]	4558.773	(0.20, 0.60, 1.00) 0.43, 0.83, ..., 2.43	−2.76			−2.52
Cr II(39)	4565.78	(0.17, 0.51) 0.34, 0.69, 1.03, 1.37	−3.24	−1.27	3	−1.87
Cr II(—)[a]	4587.306	(0.02, 0.05, 0.08, 0.11) 1.00, 1.03, ... 1.22	−1.76	−0.81	3	−1.41
Cr II(44)	4588.217	(0.07, 0.20, 0.33) 0.91, 1.04, ..., 1.57	−0.88	−0.63	4	−0.61
Fe II(38)	4541.523	(0.40, 1.20) 0.00, 0.80, 1.60	−2.93	−3.05D	2	−3.05
Fe II(38)	4576.311	(0.17, 0.51, 0.86) 0.51, 0.86, ..., 1.89	−2.89	−3.04D	2	−3.04
Fe II(38)	4583.829	(0.05, 0.14, 0.24, 0.33) 1.00, 1.10, ..., 1.67	−1.90	−2.02D	2	−2.02
Fe II(26)[a]	4583.991	(0.33, 1.00) 1.40, 2.07, 2.73	−4.48			−4.48

[a] Weak contributor to a blend.

REFERENCES.—(1) Wiese and Martin 1986; (2) Martin, Fuhr, and Wiese 1988; (3) Wujec and Weniger 1981; (4) Kostyk and Orlova 1983.

shifts) to generate integrated intensity and polarization profiles. These profiles are convolved with a triangular instrumental profile with a full width at half-power of 0.1 Å for comparison with observation.

This program has been previously used to model observations of the magnetic and spectrum variable Ap star 53 Cam = HD 65339 (Landstreet 1988). In that analysis, limitations in the available computer resources required computations to be limited to single-line profiles at one or a few phases. The calculated profiles were plotted and compared visually to plots of observations, the model field or abundance parameters were adjusted by guess, and the cycle of parameter adjustment, calculation, and visual inspection was repeated until a reasonably satisfactory agreement was achieved.

A major limitation of this approach as applied to 53 Cam was that both magnetic field geometry and abundance distributions had to be described by a very small number of parameters in order for the comparison and iteration procedure not to get out of control. The magnetic field geometry eventually used was made up of collinear axisymmetric dipole, quadrupole, and octupole components; the adjustable parameters available were the polar field strengths B_d, B_q, and B_o of the three components. The abundance distribution for each element was limited to three rings or caps of uniform abundance, axisymmetric about the magnetic axis. For simplicity, each ring was taken to have the same width (60°) in α, the colatitude measured from one of the magnetic poles. In addition, the inclination i of the rotation axis to the line of sight and the obliquity β of the magnetic field axis to the rotation axis appear as adjustable model parameters. This very coarse description of the magnetic and abundance geometries was sufficient to permit fairly satisfactory modeling of lines of (roughly uniformly distributed) Cr and Fe but was less successful for lines of (highly nonuniform) Ti.

The inefficiency of having plotting and visual inspection interposed in every step of the modeling, and the small number of model parameters that can usefully be adjusted by guess, suggested that some substantial changes should be made to the modeling procedure before another star was studied. The availability of time on a Cray X-MP/22 supercomputer at the Ontario Centre for Large-Scale Computation made it possible to contemplate changes in the line synthesis program that would substantially speed up the modeling process at the cost of a significant increase in total CPU cycles. Accordingly, the line synthesis program used to model 53 Cam was first adapted for use on the vector machine, resulting in an 80-fold speed increase relative to the Cyber 170/835 used for previous calculations. The program was then modified to read in the observed line profiles of up to three spectral lines at several observed phases, to calculate model profiles of all chosen lines at these phases, and to compute the mean square difference between the calculated and observed profiles. The calculated mean square differences were then used to choose the best radial velocity v_r and projected rotational velocity $v \sin i$. A final single numerical measure of the goodness of the model fit was then given by the residual mean square difference between observed and calculated lines (at the best values of v_r and $v \sin i$), averaged over all lines and phases.

These modifications to the line synthesis program, which provide immediate information on the quality of the fit of a given model to the observations, together with the fact that a set of line models may be computed within a couple of minutes of real time on the Cray (as opposed to overnight on the Cyber), enormously speed up the process of finding a suitable model of field or abundance geometry, even if the parameter changes are done by hand.

The availability of a numerical characterization of the goodness of fit of a given model, and the very high speed of calculation on the Cray encouraged a further development of the line synthesis program, to perform an automated search of parameter space for a best-fit model to describe the observations. This has now been implemented for fitting the abundance distribution for one element at a time to observed line profiles. The abundance distribution for each element is still assumed to be axisymmetric about the magnetic field. The continuous variation of abundance $\epsilon_Z(\alpha) = N_Z(\alpha)/N_{\rm tot}$ of the element of atomic number Z is approximated by up to six rings of uniform abundance, all of equal width in α; the abundances ϵ_{Zi} in these rings are the parameters that are varied to match the line profile. (Since the basic gridding of the visible stellar hemisphere for numerical calculation of the integrated disk line profile from those computed locally is a division into elementary regions typically 15° or more across, the resolution of the model abundance geometry—at least in one dimension—is beginning to approach the resolution set by the line synthesis program when six rings are used.)

The parameter set giving the best fit is found using an adaptation of the downhill simplex method of Nelder and Mead (1965), as programmed by Press *et al.* (1986). This method has proved to be quite effective for the present problem, as well as resonably fast; a single run searching for the best model abundance distribution of a single chemical element, using one line observed at five phases, and starting from any reasonable guessed abundance distribution, typically converges to a precision appropriate to the model in about a quarter of an hour of Cray CPU time, about the same time required for computation of a *single line profile* on the Cyber.

The actual use of these extensions of the basic line synthesis program will be described in more detail in the next section of this paper.

IV. A MODEL FOR HD 215441

a) Choice of Model Atmosphere

The line synthesis program used for profile fitting requires as input a tabulated model atmosphere, which we take from the literature, as we are not at present able to calculate our own atmosphere models. Models are available from the very large grid of Kurucz (1979), calculated for solar composition and for lower metal abundances, and from the small grid of Muthsam (1978, 1979), calculated for only a few temperatures and only for $\log g = 4$, but having composition much nearer that expected for HD 215441.

We may choose possibly appropriate models from these two grids by comparing observed photometric indices to those calculated for the model grids. For Kurucz's models, the comparison is most conveniently made using the reddening-insensitive Strömgren indices $[u - b]$, $[c_1]$, $[m_1]$, and β, which have been calculated by Lester, Gray, and Kurucz (1986) for all the published Kurucz models as well as for many unpublished ones. Minimizing the mean square deviation of the observed values of these four indices (Hauck and Mermilliod 1980) from the theoretical ones, the best-fitting Kurucz model of solar composition is found to have $T_e \approx 16{,}200 \pm 600$ K and $\log g = 4.5 \pm 0.5$. When comparison is made with the Strömgren indices of the unpublished Kurucz grid of models having

10 times the solar metal abundance (Lester, Gray, and Kurucz 1986), the best-fitting model is found to have $T_e \approx 15{,}500 \pm 700$ K and $\log g \approx 4.3 \pm 0.6$.

Comparison of the Muthsam atmosphere with observed colors may be done using either Johnson *UBV* colors or Geneva colors, both of which are computed by Muthsam. The observed mean *UBV* colors of HD 215441 (Nicolet 1978), corrected for reddening, are $(B-V)_0 = -0.19$, $(U-B)_0 = -0.64$. These colors suggest that the most appropriate Muthsam model would have $T_e \approx 14{,}600 \pm 300$ K, a value of T_e somewhat lower than that obtained from models with more nearly solar composition, as expected (cf. Stępień and Muthsam 1980). Comparison with observed Geneva colors (Rufener 1981) suggests a best T_e value of about $14{,}300 \pm 300$ K. The value of $\log g = 4.0$ assumed by Muthsam for all his models is not greatly different from the values of 4.3–4.5 derived from comparison of Kurucz models with observed colors, so in view of the high abundances expected to be present in HD 215441, we have begun by assuming that a Muthsam model of about $T_e = 14{,}500$, $\log g = 4.0$ would give a reasonable first approximation to the (mean) atmosphere of HD 215441. As no such model is available in the grid of Muthsam, we have obtained it by linear extrapolation from the two hottest models, S79 and S80 (with $T_e = 12{,}250$ and 13,750 K, respectively), taking each of the quantities σ (integrated mass surface density), T (local temperature), ρ (local mass volume density), n_e (electron number density), and τ_{5000} (optical depth at 5000 Å) at a given tabular level to be given by a simple extrapolation of the corresponding quantities at the same level using the general expression

$$y_i(14500) = y_i(12250) + [y_i(13750) - y_i(12250)] \times \left(\frac{14500 - 12250}{13750 - 12250}\right) = 1.500y_i(13750) - 0.500y_i(12250)\,, \quad (2)$$

where y_i represents any of σ, T, ρ, n_e, or τ_{5000} at level i. This leads to an apparently reasonably model not greatly different from S80 except for somewhat higher T at each level.

Note that although some data are available about broadband ultraviolet fluxes from HD 215441 (Leckrone 1974), we have selected our model without reference to these data. However, comparison of Leckrone's data with tabulated fluxes for the Kurucz model having $T_e = 16{,}000$, $\log g = 4.5$, and solar composition shows that this model is, as expected, considerably brighter in the ultraviolet than HD 215441, while the ultraviolet flux distribution of Muthsam's model with $T_e = 13{,}750$ (the main constituent of our model) is quite similar to that observed for HD 215441.

The adopted model is at best a rather crude approximation to the actual atmosphere of HD 215441, even apart from the exact values of T_e and g assumed. Although the abundance table used in constructing the models from which ours is extrapolated is fairly similar to typical abundances that we shall derive below for Si, Ti, Cr, and Fe (the only elements for which we can obtain abundances), the line profile variations observed for lines of all these elements strongly suggest that all four elements are considerably more abundant near the positive magnetic pole than around the magnetic equator, and in fact the derived abundances are mostly at least 1 dex higher near the pole than around the equator. It is thus clear that one should not use the same atmosphere model for the whole stellar surface, but should instead have models tailored to the local abundance table at each magnetic colatitude. Since the available grid of models does not permit us to do this, we have had to ignore this problem in our calculation. Consequences of this approximation will be discussed below.

b) Magnetic Field Structure

The magnetic field geometry of HD 215441 has previously been discussed by Preston (1969*a*) and by Borra and Landstreet (1978), as described in § I. Both of these papers suggest that a dipole field, inclined to the rotation axis at an obliquity β of about 30°, and viewed with an inclination i of rotation axis to the line of sight of also about 30°, provides a first, not very accurate, model of the magnetic geometry. We now try to use the available data to refine this model.

We start by extracting some important qualitative constraints from an inspection of these data. The most Zeeman-sensitive line in our spectra is the simple triplet line Si III λ4574. It is clear from Figure 1 that the separation of the σ components from the π component varies little with phase, and that the width of the σ components is not much greater than that of the π component, and is only mildly variable. There is no sign of extended wings on the σ components at any phase. These facts immediately imply that the local surface field strength $|B|$ does not vary greatly over the visible surface of the star, either on a large scale as the line of sight moves around, or on a small scale due to local field strength variations. This conclusion is of course closely related to the measured near constancy of the surface field B_s observed by Preston (1969*a*).

Both Preston's data on the relative strengths of σ_+ and σ_- components, and Borra and Landstreet's (1978) observations of circular polarization in the wings of Hβ agree in indicating that the line of sight never closely approaches the magnetic equator. The observer's line of sight never makes an angle α with the axis of the magnetic field of more than about 60° or 70°.

Now the Hβ wing circular polarization observed by Borra and Landstreet (1978), interpreted as an effective magnetic field, is quite large (up to 20.5 kG) compared to the magnitude of the typical surface field of 34 kG. The maximum effective field strength expected for a centered dipole is of the order of 40% of the surface field strength, about 14 kG in this case. The much larger maximum observed field suggests that the line of sight probably passes rather near the pole of the field, and that the field is probably not well approximated by a centered dipole, conclusions already reached by both Preston and by Borra and Landstreet. If the minimum value of magnetic colatitude α is near 0°, then the observations suggest a maximum near 60°, since the effective field is determined almost uniquely by the strength of the dipole components (cf. Fig. 4 of Landstreet 1988).

From the observed value of $v \sin i \approx 5$ km s^{-1} and the period, Preston estimates $i \sim 20°$ or 30°. This suggests as a starting model an obliquity of $\beta \sim 30°$ and an inclination of $i \sim 30°$, with a dipole field strength at the pole $B_d \sim 40$ kG or more. To allow for the possibility that the field is markedly nondipolar, we include, along with the dipole, collinear quadrupole and linear octupole components of polar strengths B_q and B_o. The models preferred by Borra and Landstreet (1978), which are given as decentered dipole models, are of this form; they are closely similar to a dipole-quadrupole expansion (cf.

Deridder, Van Rensbergen, and Hensberge 1979) with $B_d = 61$ to 73 kG, and $B_q = -37$ to -66 kG.

The Hβ Zeeman analyzer measurements of Borra and Landstreet (1978) provide important constraints on the observing geometry, especially on the values of i and β. However, as discussed by Landstreet (1988), we do not yet actually model the observed Hβ line wing circular polarization, and so we are forced to regard the Hβ observations as constraining some simple moment of the magnetic field distribution. In the previous paper (Landstreet 1988) we considered using the Hβ measurement to constrain either the effective field B_e (the average of the line-of-sight component of the field weighted by limb darkening) or the mean longitudinal field B_l (the average line-of-sight component of the field, weighted by $\cos\theta$, where θ is the angle between the local normal and the line of sight; cf. Landstreet 1982). In that paper we assumed that the Hβ observations defined the variation of B_e. We shall reconsider that choice below.

To define more exactly an appropriate model of the field and observing geometry of HD 215441, we turn to modeling of the Si III λ4574 line. This is probably the best line for constraining the field geometry in our 65 Å spectral region for several reasons. First, it has a sufficiently large Landé factor (2.00) that the π and σ components are fully resolved. Second, it has a simple triplet Zeeman pattern so that neither π nor σ components are broadened by the separation of Zeeman subcomponents. The profiles of the σ components in particular at any phase are significantly affected by the distribution of field strength over the hemisphere of the star visible at that phase, so that the σ profiles provide useful constraints on the distribution of $|B|$. Third, the line is weak enough, probably because it is formed mainly deeper in the atmosphere where the temperature is high enough to populate the (high-excitation) lower levels, that we can reproduce reasonably well the observed profiles at all phases, which is not the case for the stronger lines of Cr, Fe, and Ti that have well-defined Zeeman structure (see below). This last point is quite important because if we cannot find an abundance distribution $\epsilon(\alpha)$ that reproduces the observed profiles of a particular line at all phases, we may be sure that the local profiles and equivalent widths of that line are in error over at least some part of the star. This in turn will lead to systematic errors in our attempt to determine the field geometry using the line profile of that line as a constraint.

We may start by considering whether a simple centered dipole field model can provide an acceptable model for the magnetic field geometry. In this case, the best overall fit to the line profiles has $B_d \approx 42$ kG. Even viewing such a dipole from directly over the pole only gives $B_e = 12.6$ kG and $B_l = 16.0$ kG, well below the observed value 20.5 kG, so the line of sight must indeed pass rather near the pole. The variation of the field component measured by Hβ, from 20.5 to 10.9 kG then implies that the maximum value of $\cos\alpha$ is about 0.5, so $\alpha \approx 60°$, and $i \approx \beta \approx 30°$. The calculated σ profiles as a function of phase, even after the abundance distribution $\epsilon_{Si}(\alpha)$ has been optimized for the line, give a rather poor fit to the observations. Due to the large (factor of 2.0) change in local field strength between the equator and pole of a simple dipole, the calculated σ components are considerably wider than the observed ones, and the positions of the σ centroids change much more with phase than the observed σ centroids do. Although such a magnetic model provides a rough first approximation to the field geometry, it is not a very satisfactory one.

We next consider a combination of only dipole plus quadrupole field (equivalent to the decentered dipole geometry of Borra and Landstreet 1978). Exploration of $B_d - B_q$ parameter space quickly reveals that a somewhat larger value of B_d, together with a negative B_q at the observed pole, gives a considerably improved fit to the data. The combination of a dipole together with a quadrupole of strength $B_q \sim -0.3B_d$ gives a local field strength $|B|$ that varies by only $\pm 18\%$ from the mean over more than one hemisphere (out to $\alpha \approx 120°$), although a strong concentration of flux occurs near the opposite pole. The relative uniformity of the local field contrasts to the case of a simple, centered dipole, for which the local field varies by $\pm 33\%$ around the average.

The best fit to the λ4574 line profile is found for $B_d = 50$ kG, $B_q = -15$ kG. With these parameters, the maximum value of B_e is 14.8 kG, while that of B_l is 17.5 kG. These values are significantly closer to the observed values than those resulting from a simple dipole, but are still somewhat low.

We next consider whether the model of the field may be further improved by adding an octupole component. We have searched for the best fit to the λ4574 line in the $B_d - B_q$ parameter plane for several discrete values of B_o. The results of these experiments show that the best fit to the line profiles is found for values of B_o between roughly $+20$ kG and -20 kG, and that acceptable fits are found for $|B_o|$ as large as 30 kG. For a given value of B_d, the B_q and B_o values that give the best fit to the λ4574 line profiles are given approximately by

$$B_q = -2.0B_d + 85 \tag{2}$$

and

$$B_o = +1.5B_d - 75\,, \tag{3}$$

where all values are in kG. Acceptable fits to the line profile are found for B_d ranging from roughly 30 to 70 kG, with the optimum fit near $B_d = 50$ kG.

Because a value of B_d near 50 kG leads to values of B_e or B_l somewhat smaller than observed, and since B_e and B_l scale linearly with B_d, the constraint provided by the Hβ measurements favors larger values of B_d. A field model with $B_d = 67$ kG, $B_q = -55$ kG, $B_o = 30$ kG, and $i \approx \beta \approx 35°$ provides a reasonable compromise among the data: it fits the λ4574 line acceptably, though not as well as the model with $B_d = 50$ kG, $B_q = -15$ kG, and $B_o = 0$, and it leads to values of B_l ranging between 19.5 and 9.7 kG, in reasonably good agreement with the observed values of 20.5 and 10.9 kG. The value of B_e at the pole is still about 20% smaller than observed, however, and it appears that increasing B_d (and B_q and B_o according to eqs. [2] and [3]) enough to have B_e fit the Hβ observation will lead to calculated line profiles in rather poor agreement with the observed ones.

Thus it seems that we still have not found a really exact description of the field geometry. If we try to fit the observed λ4574 as well as possible, the calculated values of both B_e and B_l are significantly smaller than the observed field strength inferred from the Hβ Zeeman measurements, while if we increase B_d enough to fit the Hβ measurements with either B_e and B_l, we degrade the fit to the observed λ4574 profile. We finally decided to adopt the model with $B_d = 67$ kG, $B_q = -55$ kG, and $B_o = 30$ kG with $i = \beta = 35°$. This model is a reasonable compromise among the various constraints and probably does provide an approximately correct description of the field in the interval $0 < \alpha < 130°$. The predicted field strength at the unobserved pole varies greatly from one model to another, and

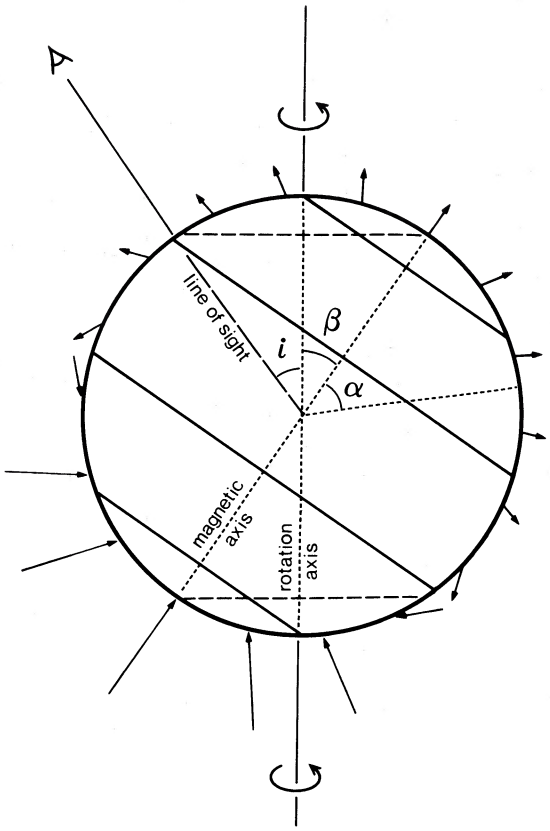

FIG. 5.—The geometry adopted to describe HD 215441. The vertical axis in the figure is the rotation axis of the star. At an angle $i = 35°$ from this axis is the line of sight. At an angle $\beta = 35°$ from the rotation axis is the axis of the magnetic field; as the star rotates the north and south poles follow the paths indicated by dashed lines around the rotation axis (or in the frame of reference of the star, the line of sight follows the upper dashed line). Angles from the visible magnetic pole are measured on the stellar surface by the colatitude α. Magnetic field vectors are shown at representative points on the surface (*short arrows*). The bands in which the abundance distribution is divided are shown as solid lines normal to the magnetic axis.

must be regarded as being essentially unconstrained by the present modeling.

The adopted field structure is shown in Figure 5, which also illustrates the relationship among the various angles used and the structure of the assumed abundance distributions.

One interesting aspect of this modeling effort is that it does suggest that, at least for HD 215441, the Hβ observations are more naturally interpreted as constraining B_l rather than B_e. Detailed modeling of the Hβ line polarization is needed to clarify this point.

c) *Modeling Abundance Distributions*

Once experimentation got underway to determine model abundance distributions for the elements which can be studied with our data, it became apparent that our ability to define unique abundance distributions is rather severely limited by several factors. These are principally (1) the fact that we cannot vary the atmosphere structure from one part of the star to another to suit the local abundances derived; (2) the low $v \sin i$ and limited resolution of our data, which combine to result in line profiles having almost no observable rotational broadening; and (3) the fact that the line of sight moves only between $\alpha \sim 0$ and $\alpha \sim 70°$, which means that the observed line profiles contain mostly information about only one hemisphere.

The problem with using a single atmosphere model to describe the entire surface of HD 215441 became apparent as soon as we tried to model a weak and a strong line of one element simultaneously. We have been unable to find abundance distributions for any elements that reproduce both strong and weak lines. Invariably a distribution can be found that fits the weaker line, but which predicts a profile for the stronger line that is too shallow by several percent for phases near magnetic pole passage ($\phi \sim 0$), although a reasonable fit to the stronger line near $\phi \sim 0.5$ can normally be obtained. The nature of the problem is obvious in the models shown in Figures 1–4.

One possibility is that the difficulty might be caused by the neglect of microturbulence. We have explored this possibility. Introducing a microturbulent velocity $v_{\rm mic}$ up to about 3 km s^{-1} changes all profiles rather little, and only marginally improves the agreement between theory and observation for the strong lines. (The cores of the strong lines do not get significantly deeper with increasing $v_{\rm mic}$, they merely get a little broader). Larger values of $v_{\rm mic}$ broaden the calculated profile and blend together the π and σ components, and for $v_{\rm mic} > 4$ km s^{-1} the agreement between theory and observation becomes unacceptable. This is evidently *not* the source of the problem, and we continue to assume that $v_{\rm mic} = 0$.

Instead, it seems likely that the problem is that the atmosphere model used in the calculations does not give a very good description of the atmosphere near the magnetic pole, where the abundances of all the measurable elements seem to be largest. This presumably leads to local intensity profiles calculated for strong lines that near the pole are not deep enough either because the $T(\tau_\lambda)$ relationship in the adopted atmosphere model is not as steep as the one that actually prevails, or because with increasing abundance the line cores are formed farther and farther out in the atmosphere where departures from LTE may become serious, perhaps deepening the lines as they do in hotter stars (Kamp 1973, 1978).

The second major problem impeding detailed modeling is the low $v \sin i$ of the star. It is small in comparison to the instrumental resolution and other broadening mechanisms; the value of $v \sin i$ determined from weak line profiles is about 7 ± 3 km s^{-1}. This has the consequence that the observed line profiles contain very little information about approaching or receding abundance structures: Doppler imaging is not possible with these data. The essential constraints provided by the observations on possible abundance distributions come only from the variation of equivalent width with phase (or with colatitude α) of several lines of each element.

Here the fact that we cannot reproduce the profiles of strong lines near $\phi \sim 0$ has an unpleasant effect. In principle, one may chose among various possible abundance distributions that correctly predict the equivalent width variations with ϕ of weak lines by using the distributions to predict variations of saturated lines. Different models will give different ratios of local strengths of weak to strong lines, so modeling strong line profiles should provide further constraint. However, for HD 215441, this constraint is not available to us, because we cannot calculate correct profiles for the strong lines. The result is a substantially decreased ability to discriminate among various possible abundance distributions.

Finally, we see less than half the possible range in α from overhead, and a part of the stellar surface is not visible at all.

This means that abundances near the strong negative pole cannot be determined, and even around the magnetic equator the abundances are somewhat uncertain. We find that if we use six zones, each 30° wide and allow four (between $\alpha = 0$ and 120°) to vary, it is usually possible to find at least two rather different distributions ϵ_{Zi} that reproduce the data almost equally well. It appears from our experiments that the data can constrain uniquely at most three values of ϵ_{Zi} for each element.

After some experimentation, we have found that if we use five bands, each 36° wide, and vary the three between $\alpha = 0$ and 108°, we obtain apparently unique solutions which describe most of the visible surface of the star. (Because of limb darkening and limb line weakening, the region beyond $\alpha = 108°$ affects the calculated profiles rather little; the abundance there is almost unconstrained, and we set it equal to the value found for the equatorial band.) We use the weakest line(s) available for each element to determine the model ϵ_{Zi}, as we can reproduce such lines quite well, and their local profiles depend only weakly on the variations in temperature structure that presumably prevent us from modeling the strong lines accurately.

d) Abundance Distribution of Silicon

Silicon is represented in our spectra by the high-excitation (19.0 eV) lines of Si III belonging to multiplet 2. Doubly ionized Si is the principal Si ion throughout the observable atmosphere, but the high excitation potential of this multiplet keeps the lower level population down until quite high temperatures are reached; the λ4574 line only becomes optically thick at line center at about $\tau_\lambda \sim 2 \times 10^{-2}$. For this reason, it may be hoped that these lines are not extremely sensitive to problems in the outer atmosphere structure due to overall abundances changes with colatitude α.

Theoretical log gf-values for all three lines of multiplet 2 are available from Kurucz and Peytremann (1975). These are in very close agreement with the NBS evaluated values (Wiese and Martin 1986) for $\lambda\lambda$4552 and 4567 after a scale change of -0.03 to the Kurucz-Peytremann data. We adopt the NBS values for $\lambda\lambda$4552 and 4567, and the rescaled Kurucz-Peytremann value for λ4574.

The abundance distribution of Si was obtained by using λ4574, the weakest of the three lines. The best-fit distribution was found by using the line synthesis program in the automatic parameter space search mode, as described in § III, using five rings of which the three between $\alpha = 0°$–36°, 36°–72°, and 72°–108° were varied. A variety of initial conditions for the search was tried; as long as the initial abundances lie in the range of $\log \epsilon_{Si} \sim -1.5$ to -3, the program had no trouble finding a good fit, and in fact, the same final $\epsilon_{Si}(\alpha)$ is found from all starting distributions. The best-fit abundance distribution found is listed in Table 3, where we give the abundances in the three bands that were varied, as well as the solar abundance (Kurucz 1981) and the abundance assumed in Muthsam's (1978) models. This distribution has been used to generate the model profiles displayed in Figure 1. (For this figure, it was necessary to select a value of $v \sin i$. We have adopted $v \sin i = 7$ km s^{-1} in all the plots.) From an examination of Figure 1, it seems that our model, while not exact, is resonably successful at reproducing the observed line profiles except near $\phi \sim 0$, where the observed lines tend to be a little deeper than those calculated.

The uncertainty in the adopted distribution may be estimated by examining the fits of individual models tried by the line synthesis program in its search for a best fit to the observations. It appears that variations from the abundances of Table 3 by as much as ± 0.4 dex can occur in individual rings without degrading any of the line profile fits by more than about a 20% increase in mean square deviation averaged over the whole line.

TABLE 3

ADOPTED ABUNDANCE DISTRIBUTION

	Log $\epsilon(\alpha)$			
Range in α	Si	Ti	Cr	Fe
0°–36°	−1.7	−3.4	−3.8	−3.4
36°–72°	−2.0	−4.2	−4.8	−3.1
72°–108°	−3.0	−4.8	−4.5	−4.1
$\log \epsilon_\odot$	−4.5	−7.1	−6.4	−4.6
$\log \epsilon_{Muthsam}$	−2.5	−5.1	−4.4	−3.0

Another test of uniqueness is to start the parameter search from a variety of initial conditions. If the initial conditions are chosen badly enough, the program can fail to converge or end up selecting a very poor fit which seems to occur at a local minimum in mean square deviation. However, if the initial conditions are within 1–2 dex of the final distribution, the model we are fitting is simple enough that the program always finds essentially the distribution of Table 3, with deviations of ± 0.3 dex or less.

It appears that we may regard the derived abundances as uncertain in individual rings by roughly ± 0.4 dex. However, two main points seem clear in spite of these uncertainties. First, the abundance of Si is higher than the solar value everywhere on the visible surface, typically by 2 dex; and second, the abundance near the positive pole is larger (by roughly 1 dex) than that around the equator.

The derived Si abundances are so high, however, that one may wonder if some important scale error in the Si abundance might be produced by non–LTE effects similar to those that occur in hotter B stars, where departures from LTE typically strengthen the observed lines at a given abundance (Kamp 1973, 1978). It is difficult to exclude this possibility on the basis of available computations. However, Kamp (1978) has shown that the increase in equivalent width of the lines of multiplet 2 due to non–LTE effects is small (less than about 20%) for $T_e < 17{,}500$ K, $\log g = 4.0$, and solar abundance. He has also suggested that the form of the curve of growth $W_\lambda(\epsilon)$ is not terribly strongly affected by non–LTE effects, so that this result may still be roughly valid at the high Si abundance that we find. An excess equivalent width of $\sim$20% due to non–LTE effects would correspond to an abundance overestimate of the order of 0.3 dex, using λ4574. On this basis, the abundance of Si is still of the order of 2.5 dex above solar, and Si still constitutes roughly 1% of all atoms by number in the atmosphere.

e) Distribution of Titanium

Five lines of Ti II are present in our spectra, but the line at 4549.62 Å is badly blended with Fe II λ4549.47 and was not modeled. The remaining four lines all have log gf-values due to Roberts, Andersen, and Sørensen (1973) that have been evaluated and slightly corrected by the NBS (Martin, Fuhr, and Wiese 1988). The values recommended by the NBS are in quite good agreement with the values given by Kurucz and Peytremann (1975). The NBS values have been adopted. (The source

of the log *gf* value adopted for the weak Cr II λ4589.91 blend with the Ti II λ4589.96 line will be discussed in § IV*f* below.) Ti II is not the dominant ionic form of Ti anywhere in the atmosphere (it typically makes up about 10^{-2} of all Ti), but the stronger lines of Ti II in our spectral region have high enough *gf*-values and low enough excitation energies that the line cores become optically thick within the first two or three levels of the tabulated atmosphere. The calculated profiles of the strong lines will therefore be very sensitive to errors in the model atmosphere at small optical depths, and we may expect some problems in fitting the lines of this element.

In fact, the same fitting problems were encountered for Ti as for Si; distributions that reproduce the weak λ4589 are only moderately successful for the three strong lines, which are all deeper near $\phi \sim 0$ than predicted by the models. We have therefore chosen a fit based on the weak line alone, which is listed in Table 3. The profiles for this model are shown in Figure 2. The model profiles fit λ4589 observations quite well (rms deviations of less than 2% for all phases but 0.783), and also fit the moderately strong line λ4563 in an acceptable fashion (rms deviations of typically 3%). The fit to the two strongest lines, λλ4533 and 4571, is definitely worse, especially near $\phi \sim 0.0$; rms deviations of up to 6% occur. However, even for these strong lines the qualitative behavior of the calculated profiles is reasonably similar to that of the observed ones. Again a very large overabundance relative to the solar case (roughly 3 dex) is found, along with a strong concentration toward the positive magnetic pole.

f) *Distribution of Chromium*

Chromium is responsible for three features in our spectra, at λλ4558, 4565, 4588. It is also a contributor to blended features at 4555 and 4592 Å which we will not model. The λ4565 line is much weaker than the other two, and because of the problems found already in mapping with strong lines, is presumably the best line to model.

Oscillator strengths for Cr II are available from the calculations of Kurucz and Peytremann (1975), and from the experimental work of Wujec and Weniger (1981). Unfortunately, the normalization of these two sources appear to differ by roughly a factor of 10, a situation already noted in the analysis of 53 Cam (Landstreet 1988). In fact, it appears (Fuhr 1987; Sigut and Landstreet 1989) that neither set of *gf*-values has a secure normalization. However, the *relative gf*-values of the two sets are in quite good agreement over the limited wavelength range of interest: the mean difference between the Wujec and Weniger log *gf*'s and those of Kurucz and Peytremann for the eight lines in common in multiplet 44 is 0.84, with a variance of only 0.03. The obvious way to obtain better oscillator strengths for Cr II is to look for a means of renormalizing the available data.

Fortunately astrophysical log *gf*-values for a few lines in the multiplets of interest have been derived from the solar spectrum by Kostyk and Orlova (1983). Fuhr (1987) has recommended this work to us as providing the best available normalization for Cr II oscillator strengths in the blue, and we have used the Kostyk and Orlova data to renormalize the oscillator strengths of Wujec and Weniger and of Kurucz and Peytremann in our spectral range.

Four lines of multiplet 44 have log *gf*-values given by Kostyk and Orlova, by Wujec and Weniger, and by Kurucz and Peytremann. The mean differences between the first two sets of log *gf*-values is -0.60 ± 0.10, in the sense that the Kostyk and Orlova log *gf*-values are more negative. We have therefore obtained our log *gf*-values, including one for the Cr II blend contributing to the Ti II feature at λ4589.9, by correcting the Wujec and Weniger values by −0.60. This procedure provides us with oscillator strengths for all the lines of interest except for the weaker of the two lines in the λ4558.7 feature. For this line we have used the four measurements of Kostyk and Orlova to renormalize the calculated log *gf*-values of Kurucz and Peytremann for multiplet 44 by +0.24.

As is the case for Ti II, the strong lines of Cr II are optically thick close to the surface, and we again found problems in trying to obtain $\epsilon_{Cr}(\alpha)$ using the strong lines at λλ4558 and 4588. We have therefore determined the best-fit abundance distribution for Cr II solely from the profiles of λ4565. When the resulting model, given in Table 3, is used to compute profiles for λλ4558 and 4588 (cf. Fig. 3) the calculations fit the observations reasonably well around $\phi \sim 0.5$ but are too weak around $\phi \sim 0.0$, where rms differences of the order of 5%–6% are found. Again a very large overabundance (about 2 dex) relative to the Sun is found, and again a concentration toward the pole appears. However, for this element, the increase in abundance going from the equator toward the pole may not be monotonic.

g) *Distribution of Iron*

Usable lines due to Fe II occur in our spectra at λλ4541, 4576, and 4583. Other lines occur in blends at λλ4549, 4555, and 4580. A weak clean line of Fe III is present at λ4596, but this line has not been classified as far as we know, and no oscillator strength is available for it.

Oscillator strengths for Fe II are available from the work of Moity (1983), which has been slightly renormalized by the NBS group (Martin, Fuhr, and Wiese 1988). These data are in good agreement with the calculations of Kurucz (1981). One very weak contributor to the λ4583.8 feature has no experimental log *gf*-value available, and the value of Kurucz is used, in spite of the fact that this is an intersystem line for which the Kurucz value may be much too small. Fe II is distributed in the atmosphere like Ti II and Cr II and for the reasons discussed above the distribution is derived using the two weakest available clean lines, λλ4541 and 4576. Good fits to these lines (cf. Fig. 4) are found with the distribution of Table 3, which also predicts line profiles that are in reasonably good agreement with observations of λ4583 near $\phi \sim 0.5$, but show rms differences of order 4% near $\phi \sim 0.0$.

It is notable that iron is overabundant relative to the Sun by only roughly 1 dex in HD 215441, and the abundance contrast between pole and equator is also somewhat less than for other elements.

V. DISCUSSION

The general level of abundance of the four elements measurable in our spectra, Si, Ti, Cr, and Fe, is quite high compared to solar abundances, in keeping with the fact that the lines of HD 215441 are stronger than those seen in normal main-sequence stars of similar temperature, such as π Cet, 30 Peg, and HR 1415 = HD 28375. The abundance excesses of Table 3 compared to solar values range from ~1 dex for Fe to ~2 dex for Si and Cr and ~3 dex for Ti. These levels of overabundance are unusually high even for Ap and Bp stars. It is notable as well that all four elements have abundances near the visible positive pole that are ~1 dex larger than those that occur around the equator. The equatorial values resemble the abun-

dance levels assumed by Muthsam (1978, 1979) for his grid of atmosphere models; since these are precisely the elements expected to contribute most to the opacity (along with H) in the atmospheres of Ap stars, it is not too surprising that we can reproduce line profiles of both weak and strong lines fairly well near $\phi \sim 0.5$, when the line of sight is near the equator. Apart from Fe, all the other elements studied by us are overabundant relative to Muthsam's abundances by ~ 1 dex near the pole, so we should expect that it would be for lines formed near the pole that our assumed atmosphere model would provide the poorest approximation to reality, and of course it is near pole passage at $\phi \sim 0$ that our theoretical models give the worst fit to observed strong lines. Apparently near the pole the atmosphere is even more peculiar than Muthsam's, with a still steeper $T(\tau)$ or possibly with significant departures from LTE. (It is probably this concentration of *all* important metallic opacity sources near the magnetic pole that leads to the very large amplitude photometric variations [up to 0.2 in U] that are observed for this star.) Furthermore, some of the variations of the observed spectrum are not simply due directly to the higher abundance of individual elements near the magnetic pole, but to the changes in atmospheric structure induced by the combination of all such abundance variations acting in concert.

Two other features of the inferred abundance distributions are notable. First, the highest abundance regions found for the already cosmically abundant elements Si and Fe are rather large; in our model the two rings out to $\alpha = 72°$ are both high-abundance regions for these elements relative to the equatorial abundances. In contrast, the polar caps of the cosmically lower abundance elements Ti and Cr are smaller; for both these elements the midlatitude (ring 2) abundances are considerably smaller than at the pole. A second, possibly significant feature of the abundance models is that all three iron-peak elements have quantitatively similar absolute abundances both near the pole and near the equator, although in the Sun Fe is roughly 2 dex more abundant than Ti or Cr. Are we seeing some sort of saturation effect?

It is interesting to use the observed value of $v \sin i$ to constrain the physical characteristics of HD 215441. Since our magnetic model indicates that $i = 30° \pm 5°$, we may use the elementary relationship

$$R/R_\odot = Pv \sin i/(50.6 \sin i)\,, \qquad (4)$$

where P is in days and $v \sin i = 7 \pm 3$ is in km s^{-1}, to find $R/R_\odot = 2.6 \pm 1.2$. Assuming $T_e = 14{,}500 \pm 500$ K, we derive $L/L_\odot = 63 \pm 41$, or $\log (L/L_\odot) = 1.8 \pm 0.4$. Now Alcock and Paczyński (1978) have found that at 14,500 K, the zero-age main-sequence luminosity has the value $\log (L/L_\odot) = 2.0$ even for Z as low as 0.01; for higher Z, the luminosity on the ZAMS is slightly larger. It seems quite probable that HD 215441 is rather close to the zero-age main sequence in the H-R diagram, and presumably the star is evolutionarily rather young. Depending on the appropriate value of Z characterizing the stellar interior, the mass of HD 215441 is probably between 3 and 4 $M_\odot$.

Finally, it is of interest to compare the derived abundance distributions to theoretical efforts to explain the nature and structure of abundance patches on Bp stars. A general model for the development of surface inhomogeneities on Ap stars due to horizontal diffusion has been presented by Michaud, Mégessier, and Charland (1981); the specific problem of supporting a substantial overabundance of Si has been discussed by Vauclair, Hardorp, and Peterson (1979) and by Alecian and Vauclair (1981), while the consequences of horizontal diffusion of this element have been examined by Mégessier (1984).

The horizontal diffusion model of Michaud, Mégessier, and Charland (1981) suggests in a general way that iron peak elements may concentrate in regions of vertical field lines, or may be uniformly distributed. The observed distributions of Ti, Cr, and Fe are consistent with this general prediction, as all are concentrated near the positive magnetic pole. (It is unfortunate that the small values i and β prevent us from observing the negative pole of the star to see whether the same elements are enhanced around both magnetic poles, or whether—as in the case of 53 Cam—some iron peak elements concentrate around only one pole.) Further calculations will be needed to determine if the observed abundance distributions are actually in agreement with the horizontal diffusion theory.

The specific case of the derived abundance distribution of Si poses more difficulties for the diffusion theory in its present state. Vauclair, Hardorp, and Peterson (1979) note that the very high abundances of Si inferred for some Bp stars are difficult to explain on the basis of radiative levitation alone, which at 14,000 K seems able to support only a mild (factor of 2 or 3) overabundance. They suggest that a nearly horizontal magnetic field, which may slow the downward diffusion of ionized Si in the upper atmosphere of a Bp star, may be required to explain the radiative support of large Si overabundances, and if this is true they predict that Si should be most overabundant where lines of force are horizontal. This problem has been reexamined with improved atomic data by Alecian and Vauclair (1981) who conclude, in agreement with the earlier work, that a 2 dex overabundance level in a 14,000 K star can be supported only with the aid of a nearly horizontal magnetic field. This is not in good agreement with our results, which suggest overabundance of 1.5 dex or more everywhere on the visible half of the star, with the highest overabundance (up to 2.8 dex, or perhaps ~ 2.5 dex after some correction for possible non–LTE effects) where field lines are *vertical*.

A further problem is apparent when our results are compared to those of Mégessier (1984). She has calculated in an approximate way the evolution of the surface Si abundance on a 14,000 K Bp star as a result of diffusion of Si with the velocities found by Alecian and Vauclair. Mégessier's basic result is that a very young star will have Si overabundance everywhere, but largest near the magnetic equator, where magnetic support is most helpful. As time goes on, the equatorial zone will gradually empty by horizontal diffusion toward the poles, until in an old Bp star the equatorial region will become largely Si-free, while a modest overabundance of 0.7 or 1 dex will remain in polar caps.

In comparing our data to this theoretical picture, a new problem (in addition to that of understanding how a very high abundance of Si may be supported at all near the pole) arises from our computed radius for HD 215441. Our data strongly suggest that the star is near the zero-age main sequence and hence quite young, so that qualitatively it should have the highest Si abundance around the equator rather than at the pole as observed. It is not clear how our data and the theoretical models may be reconciled.

This work has been supported by very helpful programming advice (particularly from Dr. J. Stacey) and much computing time from the Ontario Centre for Large-Scale Computation.

Preparation of the manuscript has been greatly facilitated by the help of Mrs. J. Calixto, Mrs. A. Brooks, and Mrs. M. Rasche. Financial support from the Natural Sciences and Engineering Council of Canada is gratefully acknowledged.

REFERENCES

Adelman, S. J. 1974, *Ap. J. Suppl.*, **27**, 203.
Alcock, C., and Paczyński, B. 1978, *Ap. J.*, **223**, 244.
Alecian, G., and Vauclair, S. 1981, *Astr. Ap.*, **101**, 16.
Babcock, H. W. 1960, *Ap. J.*, **132**, 521.
Borra, E. F., and Landstreet, J. D. 1978, *Ap. J.*, **222**, 226.
Catalano, F. A., and Renson, P. 1984, *Astr. Ap. Suppl.*, **55**, 371.
———. 1987, *Astr. Ap. Suppl.*, **72**, 1.
Deridder, G., Van Rensbergen, W., and Hensberge, H. 1979, *Astr. Ap.*, **77**, 286.
Didelon, P. 1988, preprint.
Fuhr, J. R. 1987, private communication.
Hardorp, J., Shore, S. N., and Wittmann, A. 1976, in *Physics of Ap Stars*, ed. W. W. Weiss, H. Jenkner, and H. J. Wood (Vienna: Universitätssternwarte Wien), p. 419.
Hauck, B., and Mermilliod, M. 1980, *Astr. Ap. Suppl.*, **40**, 1.
Hempelmann, A., and Schöneich, W. 1983, *Inf. Bull. Var. Stars*, No. 2549.
Jarzębowski, T. 1960, *Acta Astr.*, **10**, 119.
Kamp, L. 1973, *Ap. J.*, **180**, 447.
———. 1978, *Ap. J. Suppl.*, **36**, 143.
Kostyk, R. I., and Orlova, T. V. 1983, *Astrometriya Astrofiz.*, **49**, 39.
Krautter, A. 1977, *Ap. J.*, **216**, 33.
Kurucz, R. L. 1979, *Ap. J. Suppl.*, **40**, 1.
———. 1981, *Smithsonian Ap. Obs. Spec. Rept.*, No. 390.
Kurucz, R. L., and Peytremann, E. 1975, *Smithsonian Ap. Obs. Spec. Rept.*, No. 362.
Landstreet, J. D. 1970, *Ap. J.*, **159**, 1001.
———. 1980, *A.J.*, **84**, 812.
———. 1982, *Ap. J.*, **258**, 639.
———. 1988, *Ap. J.*, **326**, 967.
Leckrone, D. S. 1974, *Ap. J.*, **190**, 319.
Lester, J. B., Gray, R. O., and Kurucz, R. L. 1986, *Ap. J. Suppl.*, **40**, 1.
Martin, B., and Wickramasinghe, D. T. 1979, *M.N.R.A.S.*, **189**, 883.
Martin, G. A., Fuhr, J. R., and Wiese, W. L. 1988, preprint.
Mégessier, C. 1984, *Astr. Ap.*, **138**, 267.
Michaud, G., Mégessier, C., and Charland, Y. 1981, *Astr. Ap.*, **103**, 244.
Moity, J. 1983, *Astr. Ap. Suppl.*, **52**, 37.
Moore, C. E. 1945, *NBS Tech. Note*, No. 36.
Muthsam, H. 1978, *Astr. Ap. Suppl.*, **35**, 107.
———. 1979, *Astr. Ap.*, **73**, 159.
Nelder, J. A., and Mead, R. 1965, *Computer Journal*, **7**, 308.
Nicolet, B. 1978, *Astr. Ap. Suppl.*, **34**, 1.
Press, W. H., Flannery, B. P., Teukolsky, S. A., and Vetterling, W. T. 1986, *Numerical Recipes* (Cambridge: Cambridge University Press), pp. 289–293.
Preston, G. W. 1969*a*, *Ap. J.*, **156**, 967.
———. 1969*b*, *Ap. J.*, **157**, 247.
———. 1971*a*, *Ap. J.*, **164**, 309.
———. 1971*b*, *Pub. A.S.P.*, **83**, 571.
Roberts, J. R., Andersen, T., and Sørensen, G. 1973, *Ap. J.*, **181**, 567.
Rufener, F. 1981, *Astr. Ap. Suppl.*, **45**, 207.
Stępień, K., and Muthsam, H. 1980, *Astr. Ap.*, **92**, 171.
Schöneich, W., Hildebrandt, G., and Furtig, W. 1976, *Astr. Nachr.*, **297**, 39.
Sigut, T. A., and Landstreet, J. D. 1989, in preparation.
Unno, W. 1956, *Pub. Astr. Soc. Japan*, **8**, 108.
Vauclair, S., Hardorp, J., and Peterson, D. M. 1979, *Ap. J.*, **227**, 526.
Wiese, W. L., and Martin, G. A. 1986, in *CRC Handbook of Chemistry and Physics*, ed. R. C. Weast (Boca Raton: CRC Press), p. E-328.
Wujec, T., and Weniger, S. 1981, *J. Quant. Spectros. Rad. Trans.*, **25**, 167.

P. K. BARKER: Department of Physics, York University, Downsview, Ontario, Canada M3J 1A3

D. A. BOHLENDER and J. D. LANDSTREET: Department of Astronomy, University of Western Ontario, London, Ontario, Canada N6A 3K7

M. S. JEWISON: Department of Astronomy, University of Toronto, Toronto, Ontario, Canada M5S 1A7